SCIENCE CHINA
Life Sciences

•RESEARCH PAPER•

June 2018 Vol.61 No.6: 644–650
https://doi.org/10.1007/s11427-017-9275-6

Morphological properties of medial amygdala-projecting retinal ganglion cells in the Mongolian gerbil

Liju Luan[1,2], Chaoran Ren[3,4,5], Wenyao Wang[1,2], Yan Nan[1,2], Jie Gao[1,2] & Mingliang Pu[1,2*]

[1]*Department of Anatomy, School of Basic Medical Sciences, Peking University, Beijing 100191, China;*
[2]*Key Laboratory on Machine Perception, Peking University, Beijing 100191, China;*
[3]*Guangdong-Hong Kong-Macau Institute of CNS Regeneration, Jinan University, Guangzhou 510632, China;*
[4]*Guangdong Medical Key Laboratory of Brain Function and Diseases, Jinan University, Guangzhou 510632, China;*
[5]*GHM Collaboration and Innovation Center for Tissue Regeneration and Repair, Jinan University, Guangzhou 510632, China*

Received December 29, 2017; accepted January 16, 2018; published online March 19, 2018

The amygdala is a limbic structure that is involved in many brain functions, including emotion, learning and memory. It has been reported that melanopsin-expressing retinal ganglion cells (ipRGCs) innervate the medial amygdala (MeA). However, whether conventional RGCs (cRGCs) project to the MeA remains unknown. The goal of this study was to determine if cRGCs project to the MeA and to determine the morphological properties of MeA-projecting RGCs (MeA-RGCs). Retrogradely labeled RGCs in whole-mount retinas were intracellularly injected to reveal their dendritic morphologies. Immunohistochemical staining was performed to selectively label ipRGCs (MeA-ipRGCs) and cRGCs (MeA-cRGCs). The results showed that 95.7% of the retrogradely labeled cells were cRGCs and that the rest were ipRGCs. Specifically, MeA-cRGCs consist of two morphological types. The majority of them exhibit small but dense dendritic fields and diffuse ramification patterns as previously reported in RG_{B2} (95%), while the rest exhibit small but sparse dendritic branching patterns resembling those of RG_{B3} cells (5%). MeA-ipRGCs consist of M1 and M2 subtypes. The MeA-RGCs showed an even retinal distribution patterns. The soma and dendritic field sizes of the MeA-RGCs did not vary with eccentricity. In conclusion, the present results suggest that MeA-RGCs are structurally heterogeneous. These direct RGCs that input to the MeA could be important for regulating amygdala functions.

morphology properties, medial amygdala, retinal ganglion cell, Mongolian gerbil

Citation: Luan, L., Ren, C., Wang, W., Nan, Y., Gao, J., and Pu, M. (2018). Morphological properties of medial amygdala-projecting retinal ganglion cells in the Mongolian gerbil. Sci China Life Sci 61, 644–650. https://doi.org/10.1007/s11427-017-9275-6

INTRODUCTION

The amygdala is a limbic structure that is involved in many affective brain functions, including emotion, learning, and memory. This structure is one of the most extensively studied subcortical nuclei (Janak and Tye, 2015). However, most of the studies in this field have focused on the subcortical pathways and/or cortical circuitry responsible for processing affective visual information (Pessoa and Adolphs, 2010; Tamietto and de Gelder, 2010). Recent advances in identification techniques, including genetics, viral circuit tracing, and behavioral approaches, have classified approximately 30 types of retinal ganglion cells (Sanes and Masland, 2015). However, until recently, the functional roles of these RGCs in the processing of affective visual information remained largely unknown (Dhande et al., 2015). On the other hand, some early studies suggested that there are direct retinal inputs to this nucleus (Levine et al., 1991; Cooper et al., 1994; Elliott et al., 1995; Mick et al., 1993), and recent anatomical evidence revealed that melanopsin-expressing retinal ganglion cells (ipRGCs) innervate the medial amygdala (MeA) (Hattar et al., 2006). Nevertheless, the functional sig-

*Corresponding author (email: mpu@hsc.pku.edu.cn)

nificance of these connections remains to be determined. The purpose of this study was to survey the morphology of MeA-projecting retinal ganglion cells (MeA-RGCs). It was observed that the majority of MeA-RGCs were cRGCs (95.7%), and ipRGCs only contributed up to 4.3% of the retinal input to this nucleus. Most of these cRGCs exhibited small but densely branched dendritic fields (RG_{B2}-like), and less than 5% had large and sparse dendritic fields (RG_{B3}-like).

RESULTS

Retrograde injection site

RGCs projecting to the MeA were revealed via retrograde transport of CTB to the MeA of Mongolian gerbils. The location of the MeA is illustrated in Figure 1A. As depicted in the insert, the fluorescent tracer was deposited into the MeA, and the magnified micrograph revealed the tracer deposit site (Figure 1B).

General morphological properties of MeA-RGCs

Retrogradely labeled RGC cells and melanopsin-expressing RGCs were identifiable under a fluorescence microscope (Figure 2A–E). CTB-accumulating cells displayed green fluorescence (Figure 2A and C), and ipRGCs exhibited red fluorescence (Figure 2B and D). The microphotograph shows one of the quantitatively analyzed retinal areas (Figure 2C–E). MeA-projecting RGCs showed an even distribution pattern (Figure 2C). This retinal area was approximately 0.062 mm^2, and the center of the sampling area was approximately 3.5 mm from the optic disc (OD). One hundred eighty-four retrogradely labeled MeA-RGCs were identified. Among them, eight ipRGCs were double-labeled (white filled arrowhead), but three ipRGCs were not retrogradely labeled (yellow open arrowhead, Figure 2D). The merged image is shown in Figure 2E. Consequently, the MeA-RGCs on five retinas were counted and quantitatively analyzed. Together, it was observed that 95.7% were cRGCs, and 4.3% were ipRGCs. The average number of MeA-ipRGCs was significantly smaller than the number of cRGCs (P<0.001, n=5; one-way ANOVA). The local density of the MeA-RGCs was close to 2,967 mm^{-2}.

Morphological characteristics of MeA-RGCs

Somatic and axonal morphology

Two types of MeA-cRGC cells resembling RG_{B2} and RG_{B3} were identified (see detailed description below). The soma shape of both cell types was round or oval. Both cells shared similar soma diameters, which ranged from 8.75 to 16.25 μm in diameter (mean: 11.34±1.3 μm, n=90). In comparison with our previous study of the same species, the sizes of the MeA-cRGCs were twice as small as those of the alpha RGCs that innervate the dorsal raphe nucleus (22±8 μm) (Luan et al., 2011). In comparison with cells sampled from the central and peripheral retinal locations (Figure 3), little variation in soma size with retinal eccentricity was observed. The soma sizes of the MeA-ipRGCs ranged from 8.66 to 12.59 μm (10.73±1.15 μm, n=15). Most of the axons of the MeA-cRGCs were slender, but some spines and varicosities emerged from the axons. The axonal caliber ranged from 0.45 to 0.76 μm (0.56±0.09 μm, n=15) for the MeA-cRGCs. The axonal caliber of the MeA-cRGCs was significantly smaller than that of the alpha cells, which varied from 0.7 to 2 μm (1.16±0.43 μm, n=8) (P<0.001, t test) (Figure 4F).

Dendritic morphology

Three types of MeA-RGCs were observed (Figure 4). One of the most frequently encountered MeA-cRGC types had small dendritic fields that were covered by dense and branched dendritic processes. These dendritic arbors arose from 2–4 primary dendrites. The second- and third-order processes were short and slender, and most of these dendrites gave rise to many randomly branching, short and wavy dendritic processes. Dendritic spines and varicosities were distributed throughout these processes. Most of the dendritic fields were highly asymmetric (Figure 4A and B), but some cells showed symmetric dendritic fields (Figure 4C). The dendritic field diameters of the MeA-cRGCs ranged from 81.25 to 275 μm (mean: 129.18±32.87, n=90). These cells resembled previously observed RG_{B2} cells in Sprague-Dawley rats (Huxlin and Goodchild, 1997; Sun et al., 2002). The second type of MeA-cRGCs exhibited a completely different dendritic branching pattern (Figure 4D). These cells typically had 2–3 primary dendrites but only branched once or twice. The dendritic field was covered by relatively long and smooth processes. These processes occasionally overlapped in the peripheral field. Together, eight cells with similar morphological characteristics were identified. These cells resembled RG_{B3} (Huxlin and Goodchild, 1997; Sun et al., 2002). Since the majority of MeA-cRGCs were RG_{B2} and RG_{B3}, and they shared similar dendritic field sizes, the dendritic field diameters of these cells were, thus, plotted together with eccentricity (Figure 5). The third type of MeA-RGCs was ipRGCs. Both M1 and M2 were observed (Figure 2D and E). Figure 4E depicts a displaced M1 cell. This cell exhibited typical M1 morphology. The soma of this cell was displaced to the inner nuclear layer but ramified in the outermost layer of the IPL. This dendritic field size of the cell was 213 μm, and the soma size was 9.09 μm. Eighteen melanopsin-expressing cells within 4 mm of this cell were measured and analyzed (soma size, 10.87±1.24 μm; dendritic field size, 204.3±24.32 μm, n=18). Thus, the somatic and dendritic sizes of this cell were within the range of local ipRGCs.

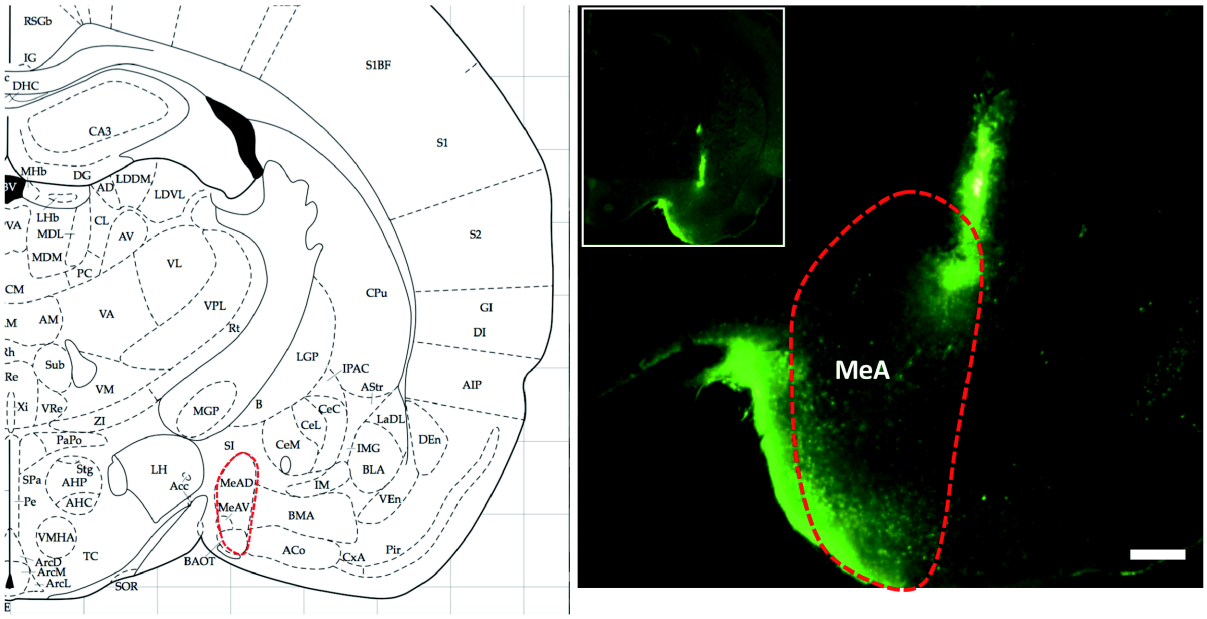

Figure 1 The medial amygdala injection site. A, The coronal section of the MeA (Paxinos, 1998). B, The MeA is revealed by the red dashed line-encircled area. Green fluorescent stain reveals the microinjection track (2.5× objective). The insert shows the micrograph of the injection site (1.25× objective). Scale bar, 500 μm.

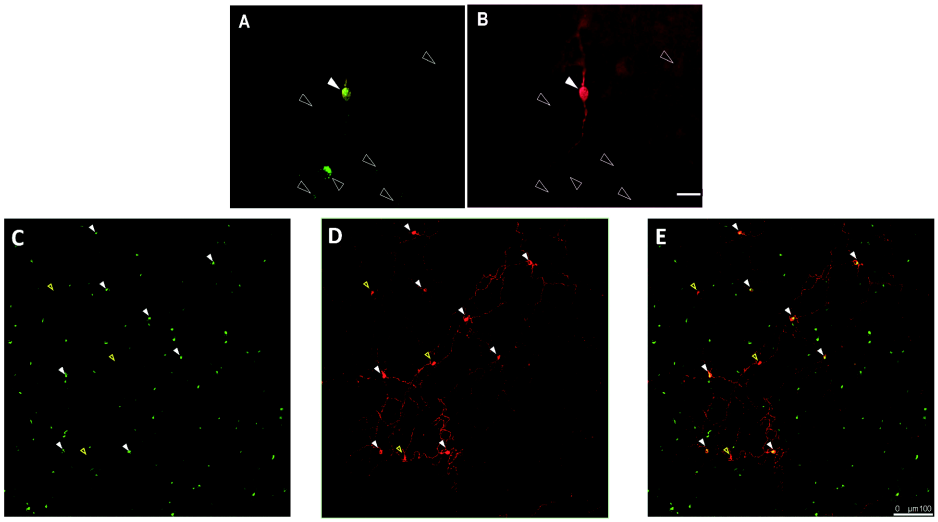

Figure 2 Retrogradely labeled MeA-RGCs and immunohistochemically stained ipRGCs. A, MeA-projecting RGCs were retrogradely labeled by CTB-488 (green). B, A melanopsin-expressing RGC (red). Open arrowheads point to retrogradely labeled MeA-RGCs; white filled arrowheads point to the double-labeled MeA-ipRGC. Scale bar, 20 μm. The retinal distribution pattern of the MeA-RGCs is revealed in C–E. C, Retrogradely labeled MeA-projecting RGCs (green). D, Melanopsin-expressing RGCs (red). E, A merged image. White filled arrowheads point to double-labeled MeA-ipRGCs and yellow open arrowheads show ipRGCs that were not retrogradely labeled. Scale bar, 100 μm.

DISCUSSION

The present study provided morphological evidence that heterogenous RGCs innervate the MeA. The majority of MeA-RGCs were cRGCs, and ipRGCs only contributed to up to 4.3% of the retinal input to this nucleus. Most of the cRGCs exhibited densely branched dendritic fields, and less than 5% had large and sparse dendritic fields. Together, the present results suggested that the MeA receives direct retinal input via both conventional and intrinsically photosensitive retinal ganglion cells.

Direct retinal projection to the amygdala

The amygdala is crucial in processing affective information (Janak and Tye, 2015; Strobel et al., 2014; Zhang et al.,

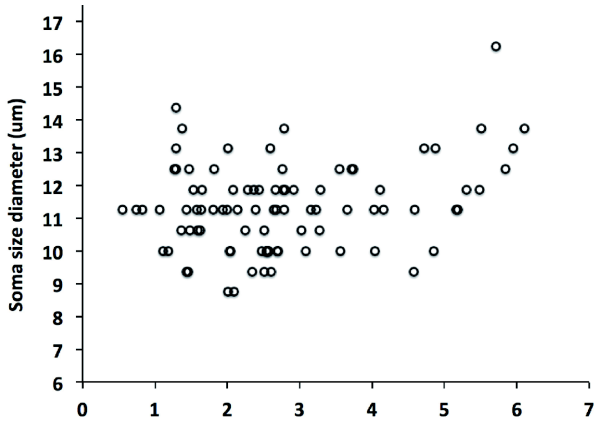

Figure 3 Soma size distribution pattern of the MeA-cRGCs with eccentricity. The vertical coordinate is the soma size (μm). The abscissa shows eccentricity (mm). Eccentricity zero represents the center of the optic disc.

2013). It has been suggested that the superior colliculus, pulvinar, and amygdala constitute a functional subcortical pathway that is essential for transferring afferent visual signals from the retina to the amygdala (Pessoa and Adolphs, 2010). Indeed, a recent study supported this hypothesis and showed that as early as 10–20 ms after the fast onset of the presentation of fearful facial expressions, an event-related synchronization in the amygdala at 20–30 ms after stimulation onset (Luo et al., 2007). In comparison, synchronization in the striate cortex occurred only 40–50 ms after stimulus onset. However, the existence of this subcortical pathway has been questioned (Tamietto and de Gelder, 2010). These authors proposed that the primary role of the amygdala in visual processing is to coordinate the function of cortical networks during evaluation of the biological significance of affective visual stimuli. On the other hand, previous studies suggested that there are direct retinal inputs that bypass the superior colliculus and the pulvinar, making monosynaptic connections with the neurons of the amygdala (Levine et al., 1991; Cooper et al., 1994; Elliott et al., 1995; Mick et al., 1993). Hattar and coworkers provided evidence that melanopsin-expressing retinal ganglion cells innervate the MeA (Hattar et al., 2006). This direct projection was recently confirmed via intraocular delivery of Cre-dependent virus (Delwig et al., 2016). However, the morphological details of RGCs innervating the MeA remained to be determined. By using retrograde tracing, intracellular injections and immunohistochemical staining, the present study provided direct morphological evidence that the MeA receives direct retinal projections from both conventional and intrinsically photosensitive RGCs. Therefore, these cells could play a major role in the processing of affective visual information.

Morphology of MeA-RGCs

The present study provided morphological evidence that heterogenous RGCs innervate the MeA. The majority of the MeA-RGCs were cRGCs, and ipRGCs only contributed to up to 4% of the retinal input to this nucleus. Most of these cRGCs exhibited small dense dendritic fields, but less than 5% had large and sparse dendritic fields. In comparison with the results of previous studies, these small, dense-field cells resembled RG_{B2} cells in rats (Huxlin and Goodchild, 1997;

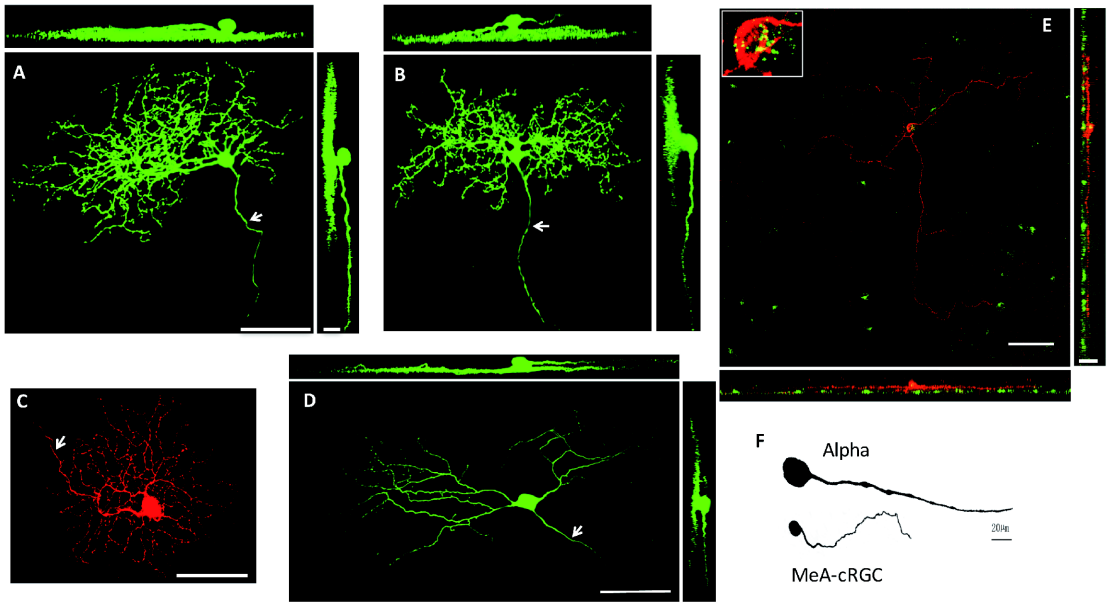

Figure 4 Dendritic morphology of the MeA-RGCs. A–D, Four intracellularly injected MeA-RGCs. A and B, Asymmetric, small and dense dendritic field cells. Scale bar for *y-z* projection, 25 μm. C, A symmetric, small and dense dendritic field cell. D, A cell with sparse and simple dendritic processes. E, A double-labeled MeA-ipRGC. This is a displaced ipRGC cell (M1 type). The insert shows a magnified micrograph of the double-labeled soma. The arrow points to the axon in A–D. Scale bar, 50 μm. F, Axon sizes of the alpha cells and the MeA-cRGCs. Scale bar, 20 μm.

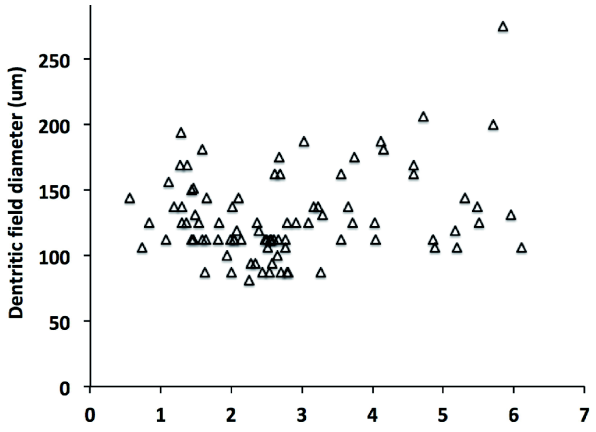

Figure 5 Dendritic field size distribution pattern of the MeA-cRGCs with eccentricity. The vertical coordinate is the dendritic field size (μm). The abscissa shows eccentricity (mm). Other conventions are as in Figure 3.

Sun et al., 2002), and similar cells were observed in mice (Sun et al., 2002), rabbits (local edge detector (LED)) (Amthor et al., 1989), and cats (zeta cell, (Berson et al., 1998)). These cells share common morphologies, including a small soma, small but dense dendritic fields, thin axons and are ramified in the middle of the IPL; presumably, these cells would be suited for slow conductance velocities and are sensitive to both ON and OFF visual signals. For MeA-ipRGCs, a previous study suggested that melanopsin-expressing retinal ganglion cells innervate the medial amygdala in mice (Hattar et al., 2006). The present study showed that only 4% of the MeA-RGCs were ipRGCs, and both M1 cells and M2 cells were identified.

Functional considerations

Based on current identification technologies, there are approximately 30 types of retinal ganglion cells (Sanes and Masland, 2015). However, until recently, the functional roles of RGCs in processing affective visual information emain sketchy (Dhande et al., 2015). The present study determined that the majority of MeA-cRGCs were RG_{B2} cells. Similar morphological profiles of RGCs have been reported in mice (Sun et al., 2002), rats (Huxlin and Goodchild, 1997; Sun et al., 2002), rabbits (Amthor et al., 1989), and cats (Berson et al., 1998). A recent study identified a W3-type retinal ganglion cell in the transgenic mouse line TYW3 (Zhang et al., 2012). These W3 cells showed LED cell morphology similar to those observed in rabbits and cats (Sun et al., 2002; Amthor et al., 1989). W3 cells have small receptive fields, respond to ON and OFF visual stimuli and are sensitive to local motion. Thus, these cells may serve as alarm neurons for overhead predators (Berson et al., 1998). It is plausible that MeA-cRGCs convey this alarm signal to the MeA and help animals escape from dangerous situations. It is intriguing that the W3 cells could detect small moving objects only if the background was featureless or stationary, whereas affective visual signals received by the MeA could have far more complex backgrounds than this. Therefore, there should be other neural circuities that convey affective visual signals to this nucleus. For instance, recently, we reported that RGCs innervate multiple non-visual nuclei (Ren et al., 2013; Zhang et al., 2012; Ren et al., 2014; Zhang et al., 2016; Huang et al., 2017); thus, eliminating these inputs could significantly, but not completely, impair the affective visual functions of these nuclei (Ren et al., 2013; Huang et al., 2017). Thus, alternative pathways could be involved in processing affective visual information. Recent developments in the use of mouse genetics, viral circuit tracing, and behavioral psychophysics have advanced the current understanding of various RGCs and their associated functions (Dhande et al., 2015). Together, these lines of evidence suggest that direct retinal inputs to these non-visual nuclei play a pivotal role in regulating affective visual functions. As such, it is plausible that these MeA-RGCs could also play a crucial role in regulating the affective visual functions of the amygdala. An ongoing study in our laboratory was designed to test this hypothesis.

MATERIALS AND METHODS

Animals

Female young adult Mongolian gerbils (*Meriones unguiculatus*) were used in this experiment. Animals were housed under a 12-hour light-dark cycle, and food and water were provided ad libitum. All experiments were performed in accordance with Peking University's guidelines for animal research and the Association for Research in Vision and Ophthalmology (ARVO) Statement for the Use of Animals in Ophthalmic and Vision Research. The animals were anesthetized (60 mg kg^{-1} sodium pentobarbital, intraperitoneally) and placed in a stereotaxic instrument. After a craniotomy was performed, a Hamilton syringe was inserted and stereotaxically positioned in the MeA. In each penetration, 0.5 μL of cholera toxin B subunit (CTB)-conjugated Alexa Fluor 488 (C34777, Invitrogen, USA) was slowly injected over 3 min. The syringe was held in place for 10 min and then withdrawn slowly. After tracer injections, the wound was sutured, and the animal was allowed to recover.

In vitro preparation

The whole-mount retinal preparation was described previously (Xia et al., 2015). Briefly, the animal was adapted to the dark for 40 min before enucleation. Under dim red light, the lens and vitreous were carefully removed with a pair of fine forceps. The eyecup was flat-mounted, sclera side down,

directly on the bottom of a recording chamber and was perfused by oxygenated (95% O_2/5% CO_2) Ames medium (Sigma-Aldrich, USA) at a fixed rate (5 mL min^{-1}) at room temperature (between 22°C–24°C).

Intracellular staining

After survival times of 3–5 days, the animal was anesthetized as described above, and the eye was enucleated and hemisected. The retina was carefully separated from the eyecup and flat-mounted on a filter paper (GS, 0.22 mm, Millipore Corp., UK) with the ganglion cell layer facing up. The retina was placed in an injection chamber and perfused with oxygenated Ames medium continually at a fixed rate (3 mL min^{-1}). Retrogradely labeled cells were filled using a microelectrode containing 4% Lucifer yellow (Invitrogen) and 3% neurobiotin (Vector Laboratories, USA). A small amount of current (1–2 nA for 1–2 min) was applied to the microelectrode until the soma and process terminals were completely stained.

Immunohistochemistry and image processes

The labeled cells were stained with anti-melanopsin. Details of the staining techniques were described elsewhere (Xia et al., 2015). Briefly, the retinas were placed in 10% goat serum in 0.3% Triton X-100 and phosphate-buffered saline mixture (Vector Laboratories) for 1 h before being incubated in a primary antibody, anti-melanopsin polyclonal antibody (PT1-780, 1:500, Fisher Scientific, USA), for 36 h at room temperature. The retinas were then placed in secondary antibodies, including Alexa Fluor 594-conjugated IgG (1:500, Invitrogen), for 2 h at room temperature. All retinas were rinsed and coverslipped with the ganglion cell side up in aqueous mounting medium (Dako Corp., USA). Ganglion cells were scanned with a confocal microscope (TCS SP5 II, Leica Microsystems, Germany). The *z*-axis interval was 0.29 μm. Each stack of optical sections covered a retinal area of 325.75×325.75 mm^2 (1024×1024 pixels). By using ImageJ and Photoshop CS5 (Adobe Corp., USA), each stack of optical sections was montaged and projected to a 0º *X*-*Y* plane and a 90º *Y*-*Z* plane to obtain a three-dimensional reconstruction of the cell. Details of the three-dimensional reconstruction and confocal calibration procedures were described elsewhere (Pu, 1999).

The method for converting intracellularly injected Lucifer yellow (Sigma-Aldrich) into permanent dye has been described previously (Ren et al., 2013). Briefly, after the injection, retinas were fixed for 1 h in 4% paraformaldehyde in 0.1 mol L^{-1} PBS at room temperature. Retinas were rinsed in 0.1 mol L^{-1} PBS three times (10 min $time^{-1}$) and placed in 10% normal goat serum containing 2% Triton X-100 and 0.5% dimethyl sulfoxide (Sigma-Aldrich) for 48 h at 4°C. Retinas were then incubated in rabbit-anti-Lucifer yellow antibody (1:1000, Sigma-Aldrich) for 48 h at 4°C. The retinas were then rinsed 3 times with 0.1 mol L^{-1} PBS and then incubated with a secondary antibody, Alexa Fluor 488 goat-anti-rabbit IgG (1:400, A-21206, Molecular Probes, USA), for 6 h at room temperature. Finally, all retinas were rinsed with 0.1 mol L^{-1} PBS and coverslipped in anti-fading aqueous mounting medium (EMS, USA).

Injection site verification

After enucleation, the animals were sacrificed with an overdose of Nembutal and perfused with physiological saline, followed by 4% paraformaldehyde. After postfixation with 4% paraformaldehyde, the brain was sectioned with a cryostat microtome (CM1900, Leica Microsystems, Germany) at 50 μm per section in the coronal plane from the anterior to posterior region of the nuclei, covering the whole length of the MeA. The sections were mounted on slides and examined under a fluorescence microscope (Zeiss Axioscop 40, Carl Zeiss, USA) to verify the injection sites and to evaluate whether the injections had invaded other visually related nuclei.

Statistical analysis

Comparisons of the dendritic field sizes and soma sizes of MeA-cRGCs with ipRGCs, and density distribution variation within the retina were analyzed using one-way ANOVA. The data are expressed as the mean±SE. The threshold for statistical significance was set at $P<0.05$.

Compliance and ethics *The author(s) declare that they have no conflict of interest.*

Acknowledgements *This work was supported by the National Nature Science Foundation of China (81401102 to Liju Luan), National Nature Science Foundation of China (31571091 to Mingliang Pu) and the National Basic Research Program of China (2016CB351806 to Mingliang Pu),*

Amthor, F.R., Takahashi, E.S., and Oyster, C.W. (1989). Morphologies of rabbit retinal ganglion cells with complex receptive fields. J Comp Neurol 280, 97–121.
Berson, D.M., Pu, M., and Famiglietti, E.V. (1998). The zeta cell: a new ganglion cell type in cat retina. J Comp Neurol 399, 269–288.
Cooper, H.M., Parvopassu, F., Herbin, M., and Magnin, M. (1994). Neuroanatomical pathways linking vision and olfaction in mammals. Psychoneuroendocrinology 19, 623–639.
Delwig, A., Larsen, D.L.D., Yasumura, D., Yang, C.F., Shah, N.M., and Copenhagen, D.R. (2016). Retinofugal projections from melanopsin-expressing retinal ganglion cells revealed by intraocular injections of Cre-dependent virus. PLoS ONE 11, e0149501.
Dhande, O.S., Stafford, B.K., Lim, J.H.A., and Huberman, A.D. (2015). Contributions of retinal ganglion cells to subcortical visual processing and behaviors. Annu Rev Vis Sci 1, 291–328.
Elliott, A.S., Weiss, M.L., and Nunez, A.A. (1995). Direct retinal communication with the peri-amygdaloid area. Neuroreport 6, 806–808.

Hattar, S., Kumar, M., Park, A., Tong, P., Tung, J., Yau, K.W., and Berson, D.M. (2006). Central projections of melanopsin-expressing retinal ganglion cells in the mouse. J Comp Neurol 497, 326–349.
Huang, L., Yuan, T., Tan, M., Xi, Y., Hu, Y., Tao, Q., Zhao, Z., Zheng, J., Han, Y., Xu, F., et al. (2017). A retinoraphe projection regulates serotonergic activity and looming-evoked defensive behaviour. Nat Commun 8, 14908.
Huxlin, K.R., and Goodchild, A.K. (1997). Retinal ganglion cells in the albino rat: revised morphological classification. J Comp Neurol 385, 309–323.
Janak, P.H., and Tye, K.M. (2015). From circuits to behaviour in the amygdala. Nature 517, 284–292.
Levine, J.D., Weiss, M.L., Rosenwasser, A.M., and Miselis, R.R. (1991). Retinohypothalamic tract in the female albino rat: a study using horseradish peroxidase conjugated to cholera toxin. J Comp Neurol 306, 344–360.
Luan, L., Ren, C., Lau, B.W.M., Yang, J., Pickard, G.E., So, K.F., and Pu, M. (2011). Y-like retinal ganglion cells innervate the dorsal raphe nucleus in the Mongolian gerbil (*Meriones unguiculatus*). PLoS ONE 6, e18938.
Luo, Q., Holroyd, T., Jones, M., Hendler, T., and Blair, J. (2007). Neural dynamics for facial threat processing as revealed by gamma band synchronization using MEG. NeuroImage 34, 839–847.
Mick, G., Cooper, H., and Magnin, M. (1993). Retinal projection to the olfactory tubercle and basal telencephalon in primates. J Comp Neurol 327, 205–219.
Paxinos, G.C.W. (1998). The rat brain in stereotaxic coordinates, 4th ed. (San Diego: Academic Press).
Pessoa, L., and Adolphs, R. (2010). Emotion processing and the amygdala: from a “low road” to “many roads” of evaluating biological significance. Nat Rev Neurosci 11, 773–782.
Pu, M. (1999). Dendritic morphology of cat retinal ganglion cells projecting to suprachiasmatic nucleus. J Comp Neurol 414, 267–274.
Ren, C., Luan, L., Wui-Man Lau, B., Huang, X., Yang, J., Zhou, Y., Wu, X., Gao, J., Pickard, G.E., So, K.F., et al. (2013). Direct retino-raphe projection alters serotonergic tone and affective behavior. Neuropsychopharmacology 38, 1163–1175.
Ren, C., Pu, M., Cui, Q., and So, K.F. (2014). Dendritic morphology of caudal periaqueductal gray projecting retinal ganglion cells in Mongolian gerbil (*Meriones unguiculatus*). PLoS ONE 9, e103306.
Sanes, J.R., and Masland, R.H. (2015). The types of retinal ganglion cells: current status and implications for neuronal classification. Annu Rev Neurosci 38, 221–246.
Strobel, C., Hunt, S., Sullivan, R., Sun, J.Y., and Sah, P. (2014). Emotional regulation of pain: the role of noradrenaline in the amygdala. Sci China Life Sci 57, 384–390.
Sun, W., Li, N., and He, S. (2002). Large-scale morophological survey of rat retinal ganglion cells. Vis Neurosci 19, 483–493.
Tamietto, M., and de Gelder, B. (2010). Neural bases of the non-conscious perception of emotional signals. Nat Rev Neurosci 11, 697–709.
Xia, H., Nan, Y., Huang, X., Gao, J., and Pu, M. (2015). Effects of tauroursodeoxycholic acid and alpha-lipoic-acid on the visual response properties of cat retinal ganglion cells: an *in vitro* study. Invest Ophthalmol Vis Sci 56, 6638.
Zhang, Y., Kim, I.J., Sanes, J.R., and Meister, M. (2012). The most numerous ganglion cell type of the mouse retina is a selective feature detector. Proc Natl Acad Sci USA 109, E2391–E2398.
Zhang, D.D., Luo, W.B., and Luo, Y.J. (2013). Single-trial ERP evidence for the three-stage scheme of facial expression processing. Sci China Life Sci 56, 835–847.
Zhang, T., Huang, L., Zhang, L., Tan, M., Pu, M., Pickard, G.E., So, K.F., and Ren, C. (2016). ON and OFF retinal ganglion cells differentially regulate serotonergic and GABAergic activity in the dorsal raphe nucleus. Sci Rep 6, 26060.